Laser−Induced InterDiffusion in AuAg Core −Shell Nanoparticles

4 AUTHORS, INCLUDING:

Jose Hodak
University of Buenos Aires
47 PUBLICATIONS **2,047** CITATIONS

Giersig Michael
Freie Universität Berlin
289 PUBLICATIONS **16,496** CITATIONS

Gregory V Hartland
University of Notre Dame
148 PUBLICATIONS **6,151** CITATIONS

Laser-Induced Inter-Diffusion in AuAg Core−Shell Nanoparticles

José H. Hodak

Department of Chemistry and Biochemistry, University of Notre Dame, Notre Dame, Indiana 46556-5670

Arnim Henglein

Notre Dame Radiation Laboratory, Notre Dame, Indiana 46556-5670

Michael Giersig

Hahn-Meitner Institut 14109 Berlin, Germany

Gregory V. Hartland*

Department of Chemistry and Biochemistry, University of Notre Dame, Notre Dame, Indiana 46556-5670

Received: July 7, 2000; In Final Form: October 3, 2000

The preparation of gold−silver nanoparticles with a core−shell structure by radiation chemistry is described. The optical properties of particles containing Au cores and Ag shells are compared to those of the reverse system for a variety of overall particle compositions. Nanosecond and picosecond laser-induced heating (at 532 nm) is used to melt the $Au_{core}Ag_{shell}$ particles into homogeneous alloyed nanoparticles. The transition from the kinetically stable core−shell structure to the alloy is demonstrated by TEM and by the spectral changes accompanying melting. It is found that the particles must accumulate many laser pulses to completely mix into the alloy. In the case of nanosecond excitation, alloying and reshaping from faceted and irregular particles into smooth spheres occurs at absorbed energies of 5−6 mJ/pulse, and fragmentation takes place at higher energies, >10 mJ/pulse. In the case of 30 ps laser excitation, the thresholds for alloying/reshaping and fragmentation are lower: 1 and 4 mJ/pulse, respectively. The higher energy threshold for nanosecond excitation compared to the picosecond case is due to dissipation of the absorbed energy to the solvent during excitation, which is estimated to occur on a 100−200 ps time scale. Thus, the temperatures reached in the particles by nanosecond excitation are lower than those achieved by picosecond excitation for equal pulse energies.

I. Introduction

The synthesis of nanometer scale materials which have controllable optical properties is of crucial importance for optical data storage applications.[1] Metal particles are robust materials that can be prepared and manipulated on the nanometer scale.[2,3] It has been demonstrated that spherical metal particles, and their aggregates, can be transformed into smaller[4−6] or larger particles[8−9] by laser excitation. The optical changes associated with these transformations provide a way of writing information to an array of nanoparticles. However, the difference in optical absorption of the system before and after this writing procedure is small, yielding a weak contrast in an eventual read step. Photoinduced reshaping of gold nanorods into spherical particles has been demonstrated to yield large spectral changes, due to the disappearance of the longitudinal plasmon band.[7,11] Thus, a high contrast ratio can be achieved in optical data storage applications. However, the large-scale synthesis of nanorods is difficult, and requires careful purification to obtain narrow distributions in aspect-ratio. For best results the orientation of the rods should also be controlled, which adds an extra step. The basis of these applications is the transformation of a kinetically stable structure (nanorod) into a thermodynamically favorable one (spherical particle) by laser-induced annealing. An interesting alternative is to use bi-metallic core−shell

particles. Two metals can be selected in such a way that the thermodynamically stable structure is an alloy which has a significantly different spectrum compared to the initial core−shell geometry. Thus, an array of core−shell particles may be used as a recording medium in optical data storage, if the core−shell particles can be transformed into alloys by optical excitation. In this scheme the alloyed particles created by laser excitation store bits of information.

In this paper we investigate laser-induced melting and alloy formation in $Au_{core}Ag_{shell}$ nanoparticles and the associated spectral changes. In addition to optical data storage applications, studies of heterogeneous nanoparticles are very important in terms of understanding the fundamental properties of catalysts, which quite often are complex structures involving different metals and their alloys. Gold−silver nanoparticles of the core−shell type have been prepared in various laboratories during the past 10 years. In the present work, the preparation of these particles using radiation chemistry is described. In this technique, particles of the core metal are made first, and the ions of the shell metal are then reduced onto the surface of the core particles. By carefully controlling the conditions for radiolysis, no reduction occurs in the absence of the seed particles. Thus, the formation of mono-metallic particles of the shell metal is avoided. It is shown that both $Au_{core}Ag_{shell}$ and $Ag_{core}Au_{shell}$ particles can be made this way. The spectra of these particles are compared at different compositions, and they are also

* Author to whom correspondence should be addressed. E-mail: hartland.1@nd.edu.

Inter-Diffusion in AuAg Core−Shell Nanoparticles

J. Phys. Chem. B, Vol. 104, No. 49, 2000 **11709**

discussed with regard to the spectra reported by other authors. For example, Sato et al.[12] reported the photochemical formation of Ag−Au composites using sodium alginate as stabilizer. They found that particles with "gold and silver domains" were formed by illumination of solutions containing both $AgClO_4$ and $HAuCl_4$; however, the exact structure of the particles was not specified. Our first report on bimetallic particles was concerned with the radiolytic formation of $Ag_{core}Au_{shell}$ structures.[13] The absorption spectra agreed fairly well with the calculated ones—small differences were thought to arise from alloy formation in an inter-facial layer. Kreibig and co-workers[14] prepared particles by chemically reducing $HAuCl_4$ or $AgNO_3$ to form the seed particles, followed by the reduction of the other salt to deposit the shell.[14−16] In all these papers, two distinct Mie peaks were observed at certain compositions of the particles. More recently, papers have appeared in which gold and silver salts were simultaneously reduced by chemical means or by radiolysis. Liz-Marzan and Philipse[17] reduced $AgNO_3$ and $HAuCl_4$ using imogolite fibers as a stabilizer and $NaBH_4$ as the reducing agent. They postulated from optical absorption measurements that they had formed bimetallic particles. The spectra did not agree with the calculated ones, and they concluded that the exact structure of the particles could not be specified. Treguer et al.[18] γ-irradiated the common solution of the two salts to obtain core−shell type structures at low dose, and alloys at high dose rates. Finally, Au−Ag alloy particles were described by Link et al.,[19,20] following the earlier work of Papavassiliou[21] and Kreibig.[15] It was found that the alloy particles exhibit a single plasmon band which is blue-shifted with increasing silver content.

In addition to investigating the spectra of the composite particles, which are unequivocally of the core−shell type, we report here on the melting of such structures upon intense laser irradiation. Both nanosecond and picosecond laser sources were used. The melting is accompanied by changes in the shape of the particles as well as in their absorption spectrum. Laser-induced melting and fragmentation of Ag[4] and Au particles[5−8,11] has previously been reported. However, several issues have not been resolved. For example, at what temperatures do melting and fragmentation occur? How does heat dissipation to the solvent affect the results of these experiments? Are the physical changes associated with melting (rod-to-sphere reshaping or alloy formation) instantaneous? The experiments reported here provide insight into these questions.

II. Experimental Section

Aqueous solutions of 20 nm gold particles were made by reducing $HAuCl_4$ by citrate, as reported by Turkevich.[22] Silver particles of 15 nm diameter were prepared by radiolytic reduction of silver ions and subsequent particle enlargement as previously described.[23] Radiolytic methods were also used to deposit the gold and silver shells.[13,24] The desired amounts of $KAu(CN)_2$ or $NaAg(CN)_2$, respectively, were added to the silver or gold sol, and the solutions were γ-irradiated under an atmosphere of nitrous oxide. The irradiation was continued until all the metal ions were reduced; this point was recognized by the complete disappearance of the UV absorption bands of the cyanide complexes. These complexes are not reduced in the absence of the seed particles. The synthesis was done in a commercial ^{60}Co source (dose rate: 8×10^2 Gy/h). The reaction vessel carried a sidearm with an optical cuvette. Spectra could therefore be measured without exposing the solution to air. After irradiation, the samples were treated with ion-exchange resin (Aldrich, Amberlite M 150) to remove the CN^- ions that were
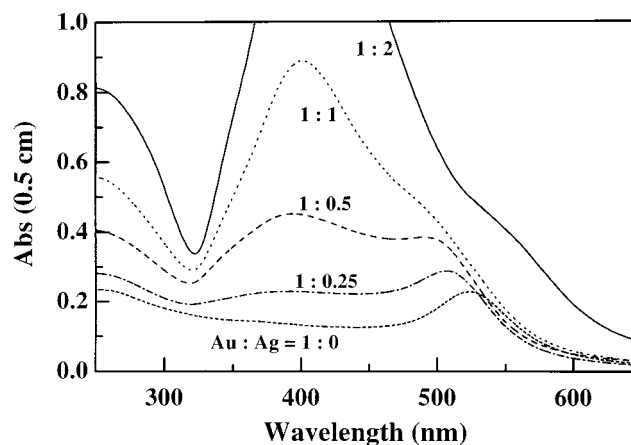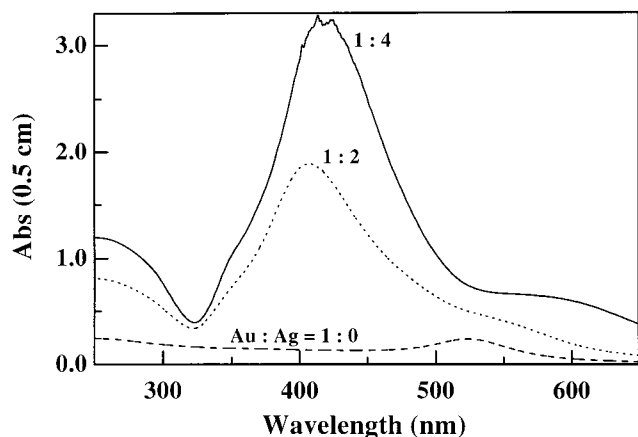

Figure 1. Absorption spectra $Au_{core}Ag_{shell}$ particles of different molar compositions. The gold concentration was 1.7×10^{-4} M, and silver was deposited in different amounts.

formed during the reduction. The samples could then be brought into contact with air. Samples for electron microscopy were prepared by putting a copper−carbon grid on a drop of the solution and letting the solution completely dry. The measurements were performed with a Phillips 12 (120 kV) or a Hitachi HF6000 (70 kV) electron microscope.

For the laser-induced melting experiments, 2.0 mL of the aqueous solution of nanoparticles was placed in a 1 cm optical path quartz cuvette. The metal concentration in the irradiated solutions was always 2.55×10^{-4} M. The solution was gently stirred while the collimated laser beam passed just above the stirrer. The solution was irradiated for 15 min, after which the absorption spectrum was collected and a TEM grid was prepared. A power-meter (Coherent 200-10) was used to measure the laser fluence with and without the sample in order to determine the power absorbed by the sample. The laser fluences stated throughout the paper are given as the absorbed energy per pulse under these experimental conditions. The laser powers are reported as absorbed rather than absolute energies per pulse, because metal particles have a complicated time-dependent spectral response to optical excitation: equal-energy nanosecond and picosecond pulses do not neccessarily produce the same level of excitation. For the nanosecond irradiation experiments a Continuum Surelite I operating at 532 nm with a pulse duration of ca. 5 ns was used. The beam diameter was 5.0 mm. In the picosecond experiments, a mode-locked Continuum PY-61 laser delivering 30 ps pulses at 532 nm was used. The beam diameter was 4.0 mm. The repetition rate was 10 Hz for both the nanosecond and picosecond experiments. The laser fluence was controlled by adjusting the current level in the flash lamps, and/or by detuning the doubling crystal. Time-resolved experiments on the picosecond time scale were performed with a regeneratively amplified Ti:sapphire laser (Clark CPA1000), with 150 fs time resolution. The details of this laser system are described elsewhere.[25]

III. Results

A. Sample Characterization: Absorption Spectra and Electron Micrographs. Figures 1−3 show absorption spectra of bimetallic particles of different compositions. The optical path length is indicated on the ordinate axis. In Figures 1 and 2 the gold nucleus had a diameter of 20 nm, and the gold concentration was 1.7×10^{-4} M. Silver shells of different thickness were deposited, keeping the overall gold concentration constant. The molar ratio $Au_{core}:Ag_{shell}$ is given on the curves.

Figure 2. Absorption spectra of $Ag_{core}Au_{shell}$ particles at higher silver depositions.
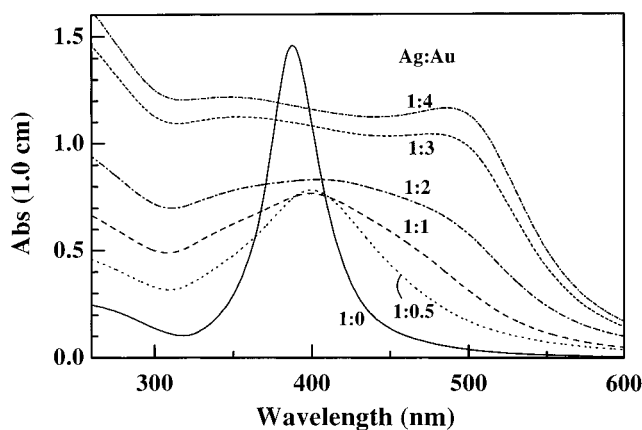
Figure 3. Absorption spectra of $Ag_{core}Au_{shell}$ particles of different molar compositions. The silver concentration was 8.5×10^{-5} M, and gold was deposited in different amounts. The absorbances are comparable with Figure 1 (note the factor of 2 in the concentrations and optical path lengths).

In Figure 3, the silver nucleus had a diameter of 15 nm and the silver concentration was 0.85×10^{-4} M. Gold shells of different thickness were deposited, keeping the overall silver concentration constant. Note that the cell thickness was twice as large in Figure 3 to compensate for the two times lower metal concentration compared to Figures 1 and 2. Thus, the absorbances between all the figures are comparable. The overall molarity of metal and the size of the particles increase with increasing deposition of the shell metal. This increase is less than a factor of 2 at the highest shell thickness. Thus, the particles are always much smaller than the wavelength of light, i.e., they belong to the size range where—according to Mie theory—the absorption spectrum is independent of particle size. Note that some authors prefer to present spectra at constant overall molarity of the two metals, assuming constant particle size. We have made silver particles with half the size of the present silver seeds and observed that the resulting $Ag_{core}Au_{shell}$ spectra did not differ from the present spectra to any noteworthy extent. The spectra in Figures 1−3 are in close agreement with the calculated ones.[16,17]

The increase in particle size upon deposition of silver onto gold seeds can be seen in the electron micrographs of Figure 4. The different panels are: Au seeds (top left), and $Au_{core}Ag_{shell}$ particles in the molar ratio Au:Ag = 1:1 (top right), 1:2 (lower left), and 1:4 (lower right). Figure 5 shows a few $Au_{core}Ag_{shell}$ particles at high resolution for the molar ratios Au:Ag = 1:1 and 1:2. The gold seeds are slightly faceted. The deposited silver

shells are also faceted. Moreover, the silver crystal does not necessarily have the facet of the original Au nucleus, which means that the growth of the silver layer occurs with different rates on the various planes of the original Au particles. The silver layer also does not have the same thickness in all particles. In fact, the micrographs in Figure 4 show a few examples where a rather small Au nucleus is in the middle of a large triangular silver crystal. The reason for this inhomogeneity is not known at this time. The increase in mean size follows the relation

$$D = D_{core}\left(1 + \frac{[Ag]V_{Ag}}{[Au]V_{Au}}\right)^{1/3} \qquad (1)$$
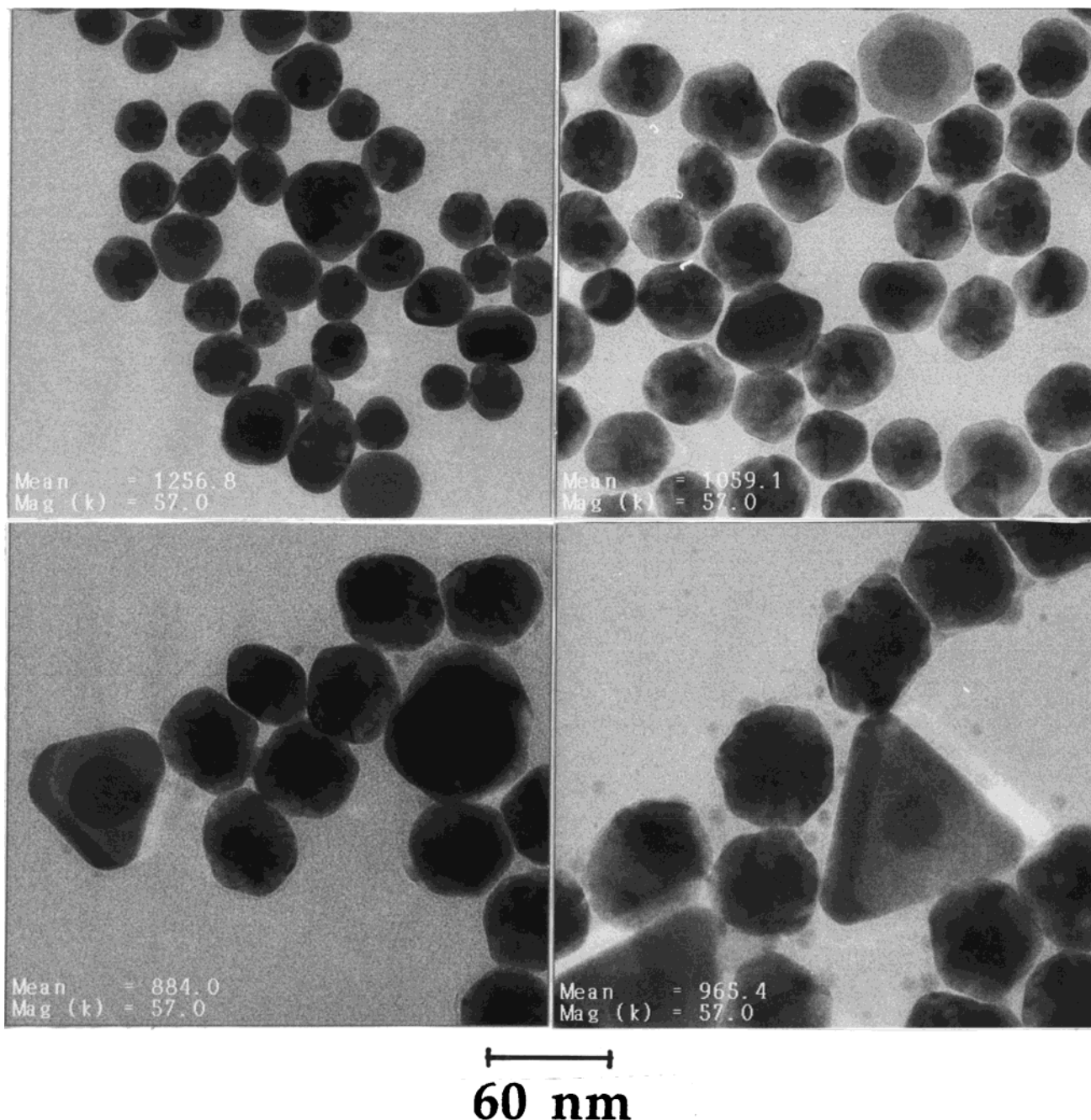
where V_{Ag} and V_{Au} are the molar volumes and [Ag] and [Au] are the overall concentrations of Ag and Au, and D is the particle diameter. These findings make it quite clear that core−shell particles have been produced. The fact that not all the particles appear to have a core−shell structure in Figure 4 is a consequence of the orientation of the nanoparticles with respect to the electron-beam in the TEM. Only under some particular conditions it is possible to achieve the necessary contrast to distinguish the two metals.

Figure 6 shows electron micrographs of $Ag_{core}Au_{shell}$ particles at low and high magnification. The chemical composition determined by energy-dispersive X-ray analysis of single particles was found to agree with the overall concentrations of the two metals in the solution. The structure of the Ag seeds has previously been investigated.[23] It was found that the seeds were mono-crystals with icosahedron and cube−octahedron shapes. Analysis of the micrographs of the composite $Ag_{core}Au_{shell}$ particles—specifically the power spectra obtained by Fourier transform of the HRTEM images—led to the conclusion that the Au forms a shell with icosahedron shape, as does the Ag core. Since both Ag and Au have cubic structure, the final conclusion is that the Au layer grows epitaxially onto the Ag seeds.[26]

Colloidal gold has a plasmon band at about 520 nm, and silver at about 380 nm. As has already been noted in former work,[12−16] these typical features of gold and silver show up in the absorption spectra of the core−shell particles, the two contributions depending on the Au:Ag ratio. Thus, it is concluded that two types of collective electron oscillations occur. The silver feature is most pronounced when Ag metal is on the outside of the bimetallic particle (see Figures 1 and 2). Specifically, a small amount of silver on the gold core (Au:Ag = 1:0.25) markedly increases the absorption at all wavelengths, with the gold plasmon band shifting from 520 to 510 nm. Upon further silver deposition, the 400 nm feature of silver develops, but pronounced increases at much longer wavelengths are also observed. At the 1:1 ratio in Figure 1, the plasmon band peaks at 405 nm and its area is much larger than that of the pure silver band in Figure 3. The coverage of silver particles with a thin gold layer (Ag:Au = 1:0.5 in Figure 3) results in a broadening and red-shift of the silver plasmon band. Further gold deposition leads to a still broader band, and the extension of the absorption into the 500 nm range, where the gold plasmon band occurs. At gold contents higher than that shown in Figure 3, the gold plasmon band develops more markedly.[13] Note that two separate maxima that correspond to the Au and Ag plasmon bands can be observed over a wide range of composition in the $Au_{core}Ag_{shell}$ particles, whereas, the silver contribution in the $Ag_{core}Au_{shell}$ particles is strongly masked by a very broad absorption below 450 nm.

B. Photoinduced Melting and Alloying. The spectra in Figure 7 show the optical changes for $Au_{core}Ag_{shell}$ particles (Au:

Inter-Diffusion in AuAg Core–Shell Nanoparticles

J. Phys. Chem. B, Vol. 104, No. 49, 2000 **11711**

Figure 4. Electron micrographs of $Au_{core}Ag_{shell}$ particles. Upper left: Au seeds; Upper right: Au:Ag = 1:1; Lower left: Au:Ag = 1:2; Lower right: Au:Ag = 1:4.

Ag = 1:0.5) induced by excitation with 532 nm, 5 ns laser pulses with different energies. As can be seen the double plasmon band characteristic of the core–shell nanoparticles disappears and a single plasmon band appears. This absorption band has a maximum between those of pure Ag or pure Au nanoparticles. The exact position of this new plasmon band depends on the composition of the nanoparticles, indicating the formation of single-phase alloyed nanoparticles. This further proves that the initial nanoparticles were indeed of the core–shell type, as opposed to a mixture of single component particles. The absorption maximum after laser treatment appears at 468 nm, i.e., close to the position found by other groups for Au:Ag 1:0.5 alloys.[19−21] Figure 8 shows the results from an experiment carried out with a 1:1 $Au_{core}Ag_{shell}$ sample. In this case the maximum absorption for the laser-treated sample appeared at 430 nm, also in fair agreement with the corresponding alloy. When the excitation is performed at high laser fluence the final

spectrum still shows a single plasmon band, but the maximum intensity blue-shifts and decreases (Figure 7d). These changes are attributed to fragmentation of the particles. Specifically, complete alloying occurs at absorbed energies >5−6 mJ/pulse, and fragmentation takes place at E_{abs} > 12 mJ/pulse. The intermediate spectrum recorded at E_{abs} = 4.6 mJ/pulse in Figure 7 (spectrum b) indicates that at this laser fluence the particles are partially alloyed.

Figure 9 shows the spectra obtained for the Au:Ag = 1:0.5 sample after irradiation with 30 ps laser pulses at different intensities. The spectra show changes similar to those observed with nanosecond excitation. The change in the morphology of the nanoparticles was monitored by TEM. Figure 10a−d shows representative pictures of the particles after 30 ps excitation. At low absorbed energies (E_{abs} = 0.13 mJ/pulse, Figure 10a) there is partial reshaping, but some core–shell particles and a significant number of faceted and oblate particles still remain
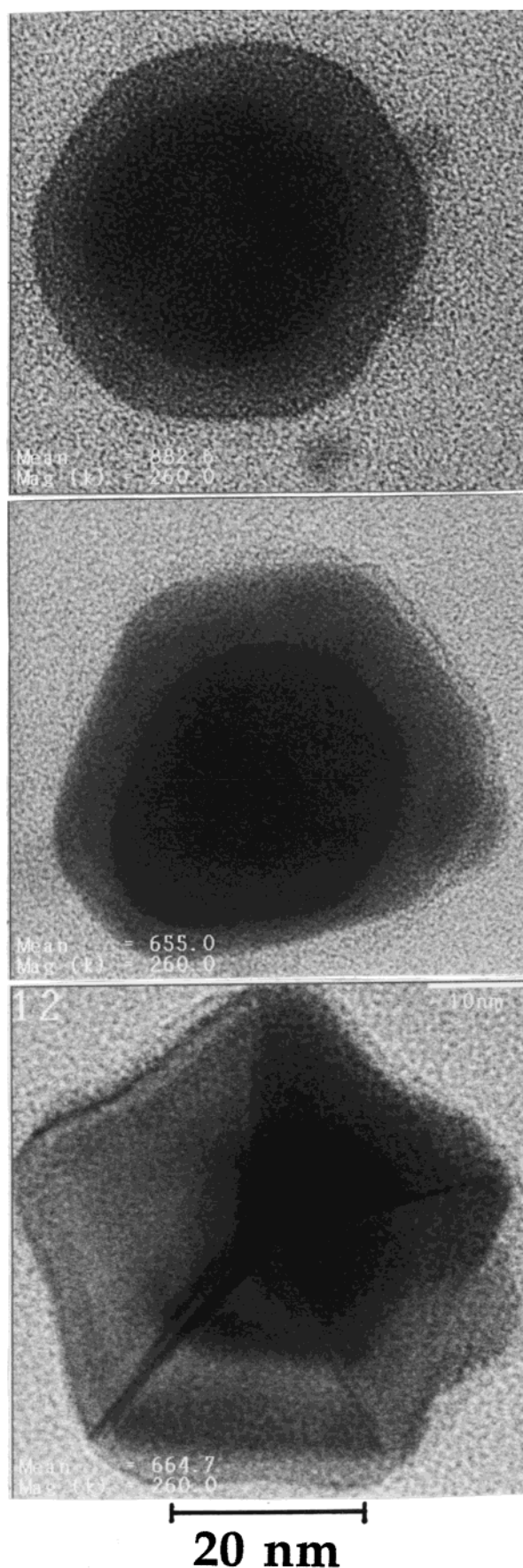
Figure 5. High-resolution electron micrographs of $Au_{core}Ag_{shell}$ particles. Upper and middle: Au:Ag = 1:1; Lower: Au:Ag = 1:2.

after 15 min of irradiation. At intermediate energies (E_{abs} = 2.05 mJ/pulse, Figure 10b), reshaping into spherical particles

is observed with complete disappearance of the core−shell structure. The resulting solution gave a spectrum similar to spectrum c in Figure 9. No signs of fragmentation are observed at this laser fluence. Notice that the narrow size distribution of the particles is emphasized by the reshaping process. At absorbed energies of 4.6 mJ/pulse (Figure 10c), both reshaping and fragmentation are observed. Similar results are obtained at higher laser fluence (E_{abs} = 6.7 mJ/pulse, Figure 10d), with an apparent reduction of the average size of the fragments. This is also evidenced in the absorption spectrum by a significant decrease in the maximum for the plasmon absorption. The reshaping and fragmentation transformations are in agreement with the results of Takami et al.[5] for pure Au nanoparticles. Note that the only difference between nanosecond and pico-second excitation appears to be that the power regime for melting and fragmentation shifts to lower laser fluence for picosecond excitation. These results are consistent with the recent study of Link et al., who compared the thresholds for melting Au nanorods with nanosecond and femtosecond laser pulses.[27] These authors found that higher laser powers must be used with nanosecond excitation to induce the rod-to-sphere transformation because of heat dissipation to the surroundings.

IV. Discussion

The 532 nm laser pulses mainly excite intra-band transitions in the Au−Ag particles. The absorbed energy is rapidly equilibrated among the electrons creating a hot-electron distribu-tion. Because the electronic heat capacity is 2 orders of magnitude smaller than the lattice heat capacity, picosecond excitation generates a substantial temperature difference between the electron gas and the lattice.[28−30] This temperature mismatch relaxes by electron−phonon (e−ph) coupling on a few pico-second time scale.[20,25,28−35] Time-resolved measurements for these core−shell particles (data not shown) indicate that the characteristic time scale for e−ph coupling is the same as that of pure Au nanoparticles.[35] Once the electrons and phonons have reached equilibrium the heat is finally dissipated into the surroundings by phonon−phonon (ph−ph) interactions.[31,32] Figure 11 shows time-resolved data for 15 and 60 nm diameter Au particles. These experiments were performed with ca. 150 fs, 400 nm pump laser pulses, and 520 nm probe pulses, with the pump laser power adjusted to give the same initial electronic temperature for both samples. The bleach recovery shows a fast and a slow component. The fast component is due to e−ph coupling and is the same for both samples (1.4 ps). The slow decay is assigned to ph−ph coupling[31,32] and is 82 ps for the 15 nm diameter particles, and ca. 200 ps for the 60 nm diameter particles. Note that (similar to the e−ph coupling time) the exact value of the ph−ph coupling time depends on the laser power. However, the time constants measured in Figure 11 are fairly typical of what is observed for Au particles in aqueous solution. These results show that the time scale for ph−ph coupling depends on the particle size—unlike the time scale for e−ph coupling.[20,34] The faster time scale for energy dissipation to the solvent for the 15 nm diameter particles is simply due to their larger surface-to-volume ratio—which enables more efficient coupling to the environment—compared to the 60 nm diameter particles.

Assuming that the heat transfer coefficients for Ag and Au are similar,[36] the time scales for ph−ph coupling for the core−shell particles should be the same as that of the pure Au nanoparticles (given that the particles have the same size). Thus, for the particles examined in this paper, the energy deposited by the laser pulse should be dissipated to the solvent on a time scale of 100−200 ps. The nanosecond and picosecond experi-
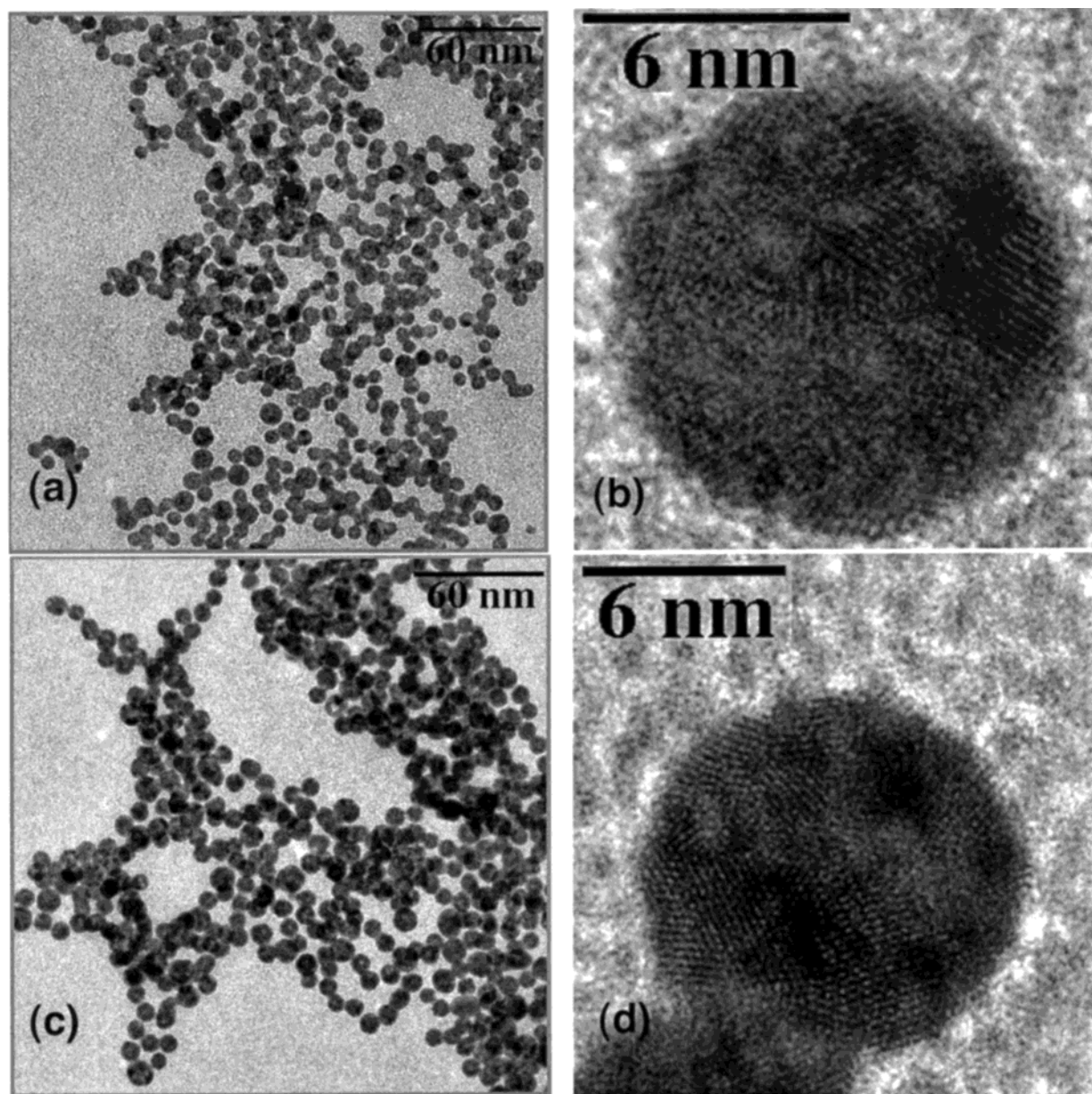
Figure 6. Electron micrographs of $Ag_{core}Au_{shell}$ particles in molar ratio Ag:Au of (a,b): 1:1; (c,d): 1:3. Note the enlargement of the particles as the Au shell becomes thicker (panels (a) and (c)) as well as the resolution of the lattice planes (panel (b) and (d)). The power spectra indicate that Au grows epitaxially onto the silver seeds.

ments described above, therefore, represent two different limits for heating the particles. In the nanosecond experiments the duration of the excitation pulse is much longer than the heat dissipation time, whereas, the picosecond pulses are much shorter than this time scale. Both laser pulses have a much longer duration than the e−ph coupling process.

In their initial report of laser-induced melting of metal particles, Takami and co-workers estimated the temperatures produced by laser excitation by neglecting energy dissipation.[5] They found that when the final temperature is lower than the boiling point, the temperature after the laser pulse is

$$T = 298 + \frac{E_{abs}}{C_p} \quad T < T_{melt} \tag{2}$$

$$T = 298 + \frac{E_{abs} - \Delta H_{melt}}{C_p} \quad T_{melt} < T < T_{boil} \tag{3}$$

In these equations ΔH_{melt} and C_p are the specific enthalpy for

melting and the heat capacity of the particles respectively, and E_{abs} is the absorbed energy per pulse and per gram. For the core−shell particles used here, these thermodynamic functions were assumed to be those of an ideal mixture of Au and Ag. When enough heat has been added so that the particles have both melted and vaporized completely, the specific enthalpy of vaporization ΔH_{vap} has to be subtracted in the numerator of the second term of eq 3. We do not reach this limit in our experiments. Note that when the temperature calculated with eq 2 is above the melting point, but not enough energy has been added to completely melt the particles, the system is considered to be at the melting point. The same holds for eq 3 when the calculated temperature is above the boiling point. The temperatures calculated for the particles based on eqs 2 and 3 are presented in Table 1. These results are very close to the initial temperatures expected for the picosecond experiments, i.e., prior to the heat transfer to the solvent (vide infra). In the nanosecond experiments, the maximum temperature obtained will be lower
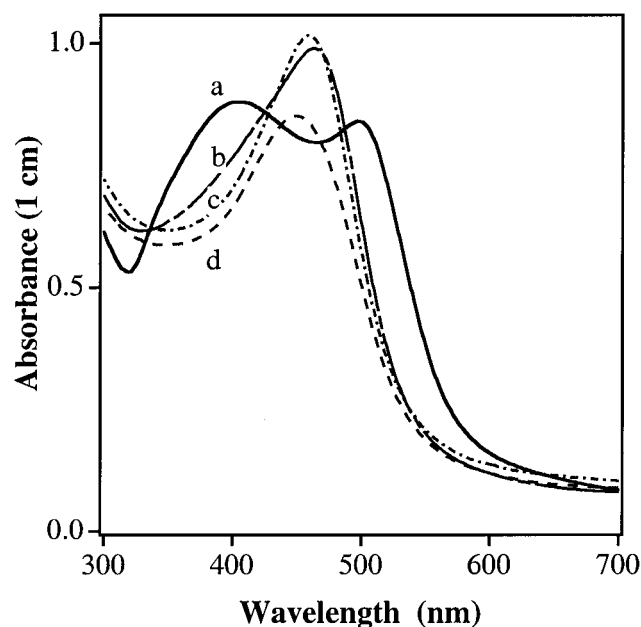
Figure 7. Absorption spectra of $Au_{core}Ag_{shell}$ particles (molar ratio Au: Ag = 1:0.5) following photoexcitation with 5 ns laser pulses at 532 nm: (a) non irradiated; (b−d) E_{abs} = 4.6, 5.6, and 12.8 mJ/pulse, respectively.

than this prediction, because significant heat dissipation takes place during the excitation.

The balance between the excitation pulse-width and the time scale for energy dissipation to the solvent can be examined by using Newton's law of cooling for energy exchange between the electrons and the lattice of the particles, and between the lattice the surroundings.[28−35] This model consists of the coupled differential equations

$$\frac{\partial T_e}{\partial t} = -\frac{g}{C_e(T_e)}(T_e - T_l) + F(t) \tag{4}$$

$$\frac{\partial T_l}{\partial t} = \frac{g}{C_l}(T_e - T_l) - \frac{T_l - 298}{\tau} \tag{5}$$

where T_e and T_l are the electronic and lattice temperatures, g is the electron−phonon coupling constant, C_l and $C_e(T_e)$ are the lattice and electronic heat capacities, $F(t)$ is the source term (i.e., the laser pulse), and τ is a phenomenological time constant that accounts for heat dissipation to the solvent. The temperature-dependent electronic heat capacity is given by $C_e(T_e) = \gamma T_e$, where $\gamma = 66$ J K^{-2} m^{-3} for Au.[37] In this model, heat is deposited into the electrons by the laser pulse, the electrons equilibrate with the phonons on a time scale determined by C_e/g, and the hot electron/phonon system then equilibrates with the surroundings. This model does not allow direct coupling between the electron gas and the environment.

Example calculations of T_e and T_l for nanosecond and picosecond excitation sources are shown in Figure 12. The parameters used in these calculations were chosen to mimic 20 nm diameter Au particles with an absorbed energy of 2.05 mJ/ pulse and τ = 200 ps. Clearly, the temperatures obtained for nanosecond excitation are much lower than those for picosecond excitation. It is noticeable that for nanosecond excitation the temporal envelope of T_e (dotted line) has the shape of the laser pulse, and the temporal evolution of T_l (solid line) closely follows that of T_e. This is in contrast to the picosecond excitation case, where the electronic and lattice temperatures evolve very
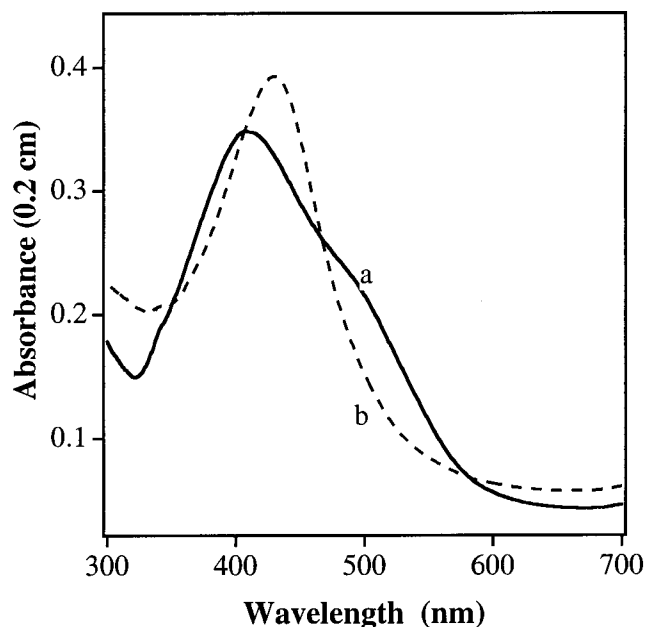
Figure 8. Absorption spectra of $Au_{core}Ag_{shell}$ (molar ratio Au:Ag = 1:1) before (a) and after (b) photoexcitation with 5 ns laser pulses at 532 nm. The absorbed energy was 3.2 mJ/pulse.
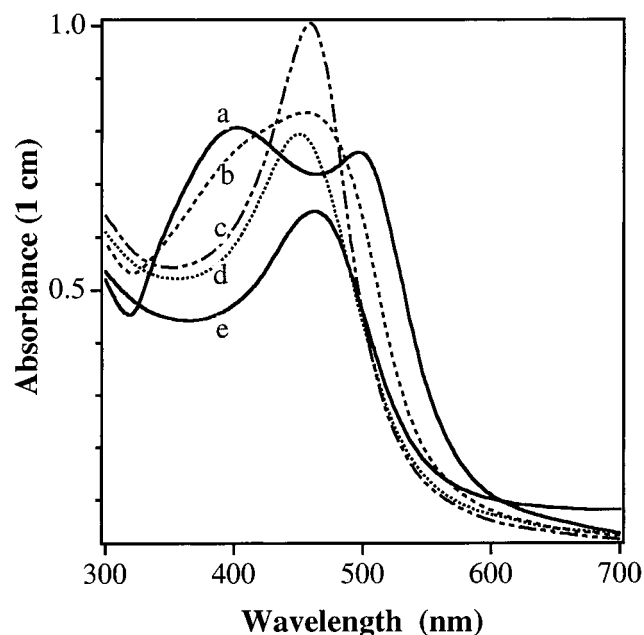

Figure 9. Absorption spectra of $Au_{core}Ag_{shell}$ particles (molar ratio Au: Ag = 1:0.5) following photoexcitation with 532 nm, 30 ps laser pulses: (a) non irradiated; (b−e) E_{abs} = 0.13, 1.16, 4.6, and 6.7 mJ/ pulse.

differently at early times. The lattice temperature immediately after the picosecond pulse is very close to that calculated with eqs 2 and 3 (i.e., ignoring dissipation). This temperature increase subsequently decays on a time scale determined by τ.

Our experiments can be viewed as a sequence of heating and dissipation processes: the peak lattice temperature is determined by the ratio of the laser pulse duration to the energy-dissipation rate. For picosecond excitation the rate-determining step for thermalization is the energy dissipation to the solvent. As a consequence, the absorbed energy is "stored" in the lattice as a temperature increase and/or a phase change. In contrast, for nanosecond excitation the relatively slow rate at which the energy is fed into the system means that the electron gas can communicate with the surroundings faster than it is excited.

Inter-Diffusion in AuAg Core−Shell Nanoparticles

J. Phys. Chem. B, Vol. 104, No. 49, 2000 **11715**
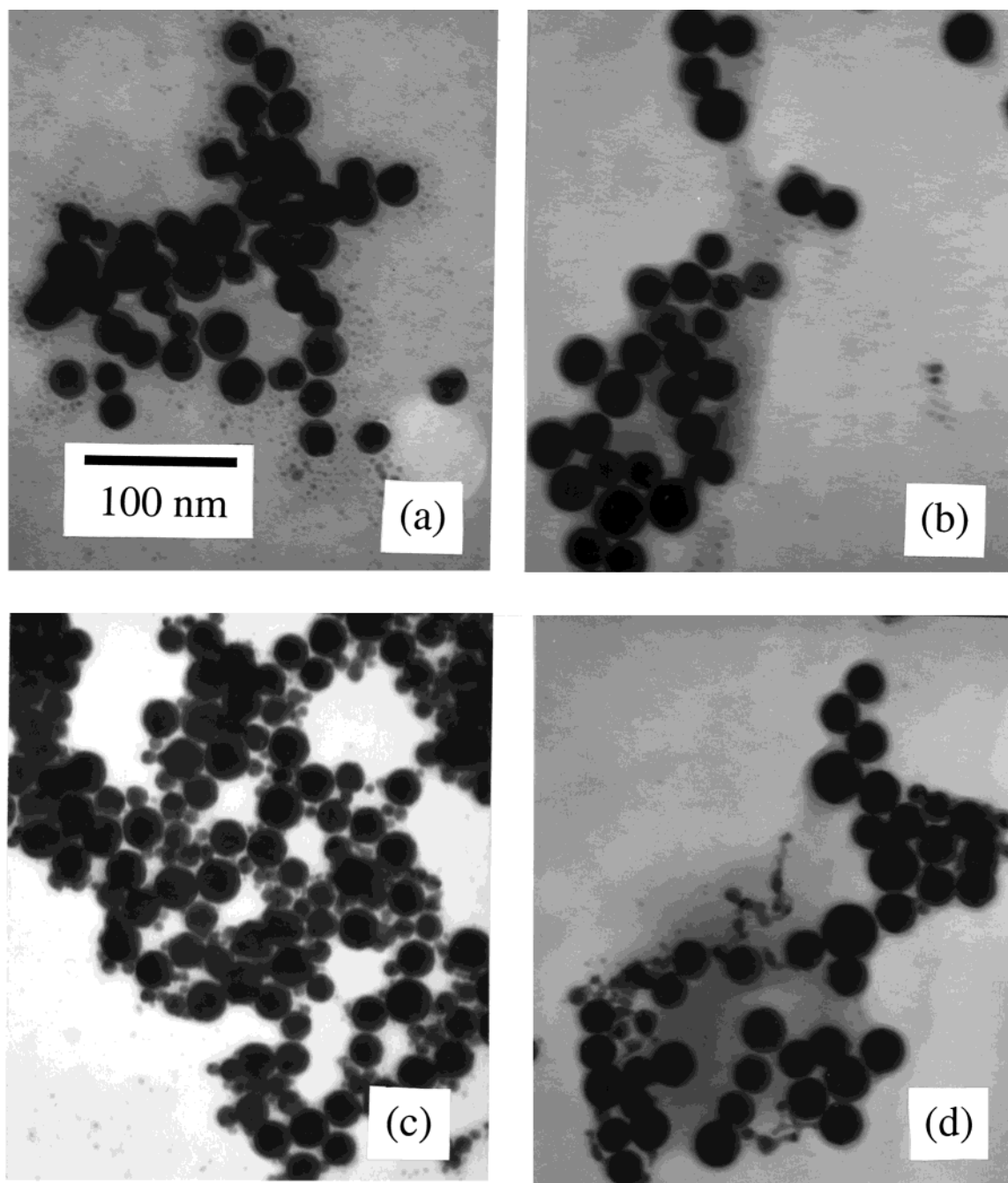
Figure 10. TEM pictures for Au$_{core}$Ag$_{shell}$ particles (molar ratio Au:Ag = 1:0.5) after irradiation with 532 nm, 30 ps laser pulses. The absorbed energies from (a) to (d) are 0.13, 2.05, 4.6, and 6.7 mJ/pulse. The total width of each panel is 380 nm.

Thus, for nanosecond excitation the electron gas and the lattice do not deviate as strongly from thermal equilibrium with the surroundings. This means that more energy per pulse is required to reach a given lattice temperature for a nanosecond excitation source. For a ph−ph coupling time of 200 ps, our calculations show that ∼20 times more energy is needed to heat the lattice to 1000 K for a 5 ns pulse compared to a 30 ps pulse. This analysis qualitatively agrees with our experimental observations: the particles become alloyed at E_{abs} = 1.1 mJ/pulse for picosecond excitation, whereas absorbed energies of greater than 5 mJ/pulse are needed to achieve similar spectral changes for nanosecond excitation. Note that for the nanosecond experiments the calculated lattice temperatures depend critically on the exact value of the ph−ph coupling time. Furthermore, when a significant amount of energy has been transferred from the particles, the temperature of the surroundings increases. This

decreases the driving force for energy flow from the particle and, therefore, the effective ph−ph coupling time.[36] This effect, and the heat diffusion in the solvent, have been left out of our calculations. Thus, the predicted temperatures based on eqs 4 and 5 are are only approximate. However, the calculations clearly demonstrate that heat dissipation to the solvent limits the efficiency of nanosecond laser sources for melting nanoparticles.[27]

It is known that Au and Ag form nearly ideal solid solutions at all compositions.[38] Therefore, mixing of the two metals is a thermodynamically favorable process. Phase diagrams for bimetallic nanoparticles have recently been calculated[39] by including the size dependence of the melting temperatures[40−42] on the thermodynamic expressions for the liquidus and solidus curves. This size dependence is due to the increase in free energy caused by the surface curvature of small particles. We have done
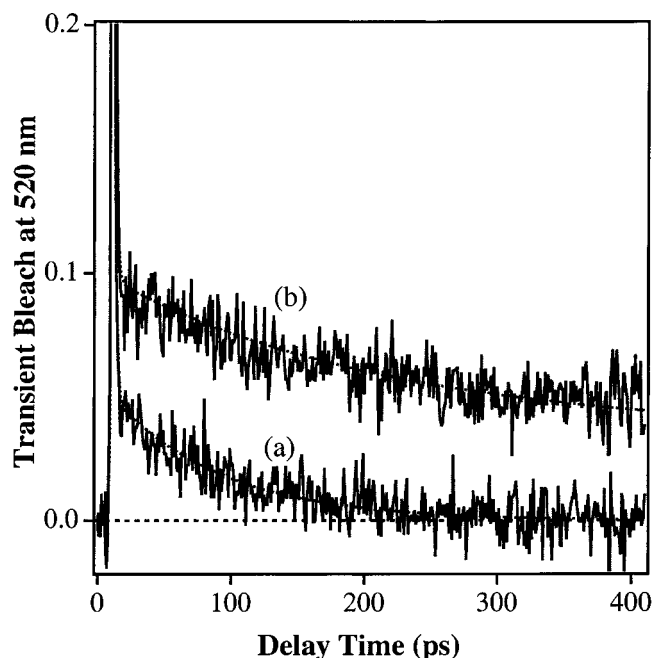
Figure 11. Time-resolved data for (a) 15 nm diameter and (b) 60 nm diameter Au particles collected with 400 nm pump, 520 nm probe pulses. The fast initial bleach recovery is due to e−ph coupling. The remaining slowly varying signal is assigned to energy dissipation to the surrounding solvent. The dashed lines are biexponential fits to the data.

TABLE 1: Temperatures Calculated Using Equations 2 and 3 for Au:Ag = 1:0.5 Nanoparticles after Excitation with 532 nm Laser Pulses; The Absorbed Energies Correspond to Those Used in the Picosecond Laser Experiments, See Text for Details

E_{abs}(mJ/pulse)	calculated temp (K)	phase
0.125	435	s
0.350	691	s
1.16	1100	s $\rightleftharpoons$ l
2.05	2161	l
2.95	2880	l $\rightleftharpoons$ v
4.60	2880	l $\rightleftharpoons$ v
6.70	2880	l $\rightleftharpoons$ v

these calculations for 20 nm diameter particles, and find that T_{melt} (Ag) = 1098 K, T_{melt} (Au) = 1229 K, and T_{melt} (Au:Ag = 1:0.5) = 1184 K. These temperatures are not significantly different from the bulk melting temperatures of Ag and Au and their mixtures. In TEM studies of melting of Pb nanoparticles it was found that a liquid mantle surrounding a solid core is formed before complete melting takes place.[43] Thus, on the basis of these data, melting for our core−shell nanoparticles is expected to start on the silver shell at about 1100 K. At higher temperatures, melting and dissolution of the core into the liquid phase will occur. Note that the calculations are based on parameters for the metal−vacuum interface. No attempt has been made to include the Au/Ag interface or the fact that the particles are in water rather than vacuum.

The TEM pictures in Figure 10 show that at least partial reshaping of the particles occurs at every laser power used in our experiments. This means that surface melting begins at much lower temperatures (ca. 430 K, see Table 1) than the melting points calculated above. These results are consistent with several recent studies of surface melting in noble metal nanoparticles. For example, in their laser heating experiments with Au particles, Takami et al. calculated that reshaping occurs at temperatures that are much lower than the expected melting point for the particles.[5] In addition, Wang and co-workers have
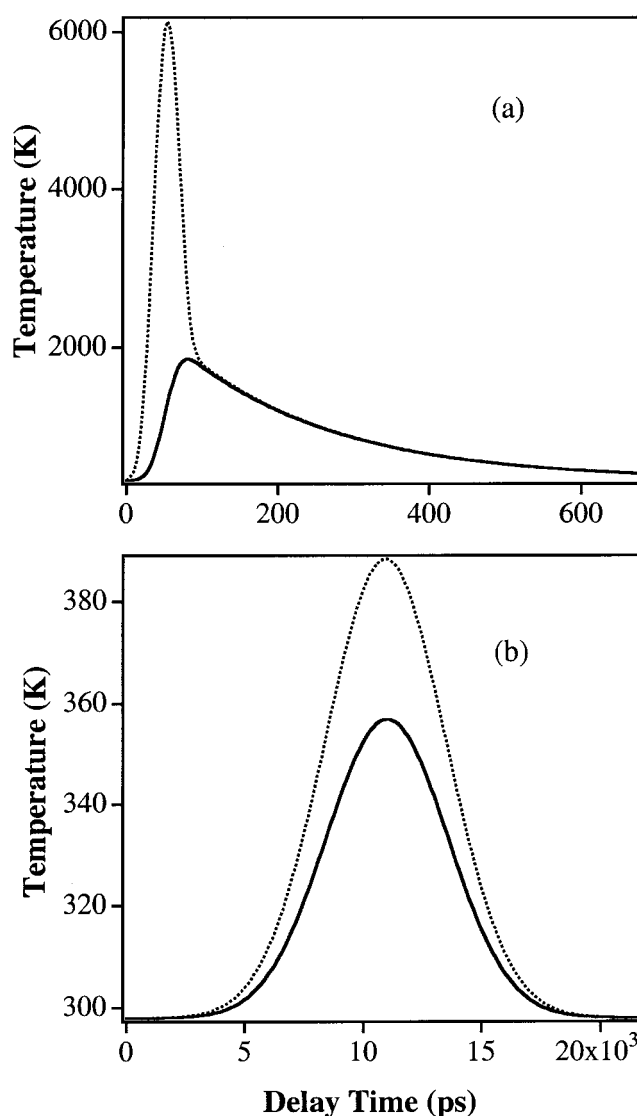
Figure 12. Temporal evolution of T_e (dotted line) and T_l (full line) calculated with eqs 4 and 5 for 20 nm Au particles excited with (a) 30 ps and (b) 5 ns laser pulses with E_{abs} = 2.05 mJ/pulse. See text for details.

used in situ TEM measurements to study shape transformations of Pt nanoparticles and Au nanorods. These workers also find that surface melting occurs at much lower temperatures than expected.[44,45] Specifically, the Pt particles show surface melting at ca. 800 K, which is significantly lower than the melting point of bulk Pt (2045 K).[44] Likewise, the Au nanorods display surface melting at ca. 500 K, again much lower than the melting point of bulk Au (1337 K).[45]

Inspection of the spectra in Figure 9 indicates that for the picosecond experiments significant alloying starts when the absorbed energies are about 0.35 mJ/pulse. At this laser fluence the temperature calculated with eq 2 is approximately one-half of the expected melting temperature for the system (see Table 1). Since this calculation ignores energy dissipation, it constitutes an upper bound for the temperature, although the initial lattice temperature in the picosecond experiments should be very close to the temperatures calculated by eqs 2 and 3. Thus, inter-diffusion of Ag and Au in the core−shell nanoparticles also occurs at temperatures that are *much lower* than the expected melting point. It is important to note that alloy formation does not occur unless the particles are exposed to the laser beam.

A significant question in these studies is whether the particles

Inter-Diffusion in AuAg Core—Shell Nanoparticles

J. Phys. Chem. B, Vol. 104, No. 49, 2000 **11717**

become alloyed under the effect of a single laser pulse, or a series of melting—solidification sequences occur with increased mixing for every laser shot. The melting of the nanoparticles occurs on the time scale for propagation of an acoustic wave across a distance equivalent to one particle diameter.[11] For our samples this is about 15 ps. On the other hand, the time scale for mixing the metals is determined by the time needed for an individual atom to diffuse over a distance equal to the radius of the particle. This time is given by $t = (R^2/6D)$, where R is the particle radius, D is the diffusion constant, and the factor of 6 arises because this is a 3D problem.[36,46,47] Because the self-diffusion constants of Ag and Au are identical,[47] the inter-diffusion constant for the Au/Ag mixture was taken to be the same as the self-diffusion constants. Thus, the appropriate diffusion constant for our system is

$$D = D_0 \exp(-E_d/kT) \qquad (6)$$

where $D_0 = 0.04$ cm²/s and $E_d = 1.76$ eV.[46] Using these parameters, the time scale for mixing is calculated to vary from seconds ($E_{abs} = 0.35$ mJ/pulse, $T = 690$ K) to microseconds ($E_{abs} = 1.16$ mJ/pulse, $T = 1100$ K). Given that heat dissipation to the solvent occurs in ca. 100—200 ps, it is very unlikely that the particles will fully mix in a single laser shot—for either picosecond or nanosecond excitation. The extremely rapid cooling also means that supercooled liquid particles—which have been observed for lead nanoparticles in a vacuum[43]—will not have a significant lifetime under our experimental conditions.

The differences between the spectra for the Au$_{core}$Ag$_{shell}$ and the alloyed nanoparticles (shown in Figures 7—9) indicate that if alloying does occur in a single laser shot, then an absorption at ca. 450 nm and a permanent bleach in the range of 490—520 nm should both be observed after the laser pulse (for a Au:Ag = 1:0.5 composition). An attempt to collect time-resolved data in the sub-nanosecond or microsecond time scales in the laser fluence range shown in Table 1 yielded negative results, indicating that single-shot laser-induced transformation does not occur. Only at a laser fluence 1 order of magnitude higher than those indicated in Figure 10 was it possible to obtain a transient signal. In this last experiment, a permanent bleach was observed in the 460—500 nm range, indicating fragmentation of the nanoparticles. Thus complete alloying does not occur in a single laser pulse. Each time the particles are exposed to a laser pulse, partial melting and inter-diffusion of the two metals takes place. Under the experimental conditions reported here, each particle will suffer an average of 700 of these annealing processes during the irradiation time. Note that fragmentation does seem to take place in a single laser shot in these systems.

It is interesting to use the observation that the particles are completely alloyed in 700 laser shots for $E_{abs} \geq 1.16$ mJ/pulse to estimate an effective inter-diffusion constant. Assuming that the temperature increase in the particles is maintained for 100 ps, then the total time that the particles remain at an elevated temperature in the picosecond experiments is $t = 70$ ns. The diffusion constant can be calculated by $D = (R^2/6t)$, where R is the particle radius (as discussed above). Using $R = 10$ nm yields $D \approx 2 \times 10^{-6}$ cm²/s. This value is between the typical values for the diffusion constants of *fcc* metals near their melting points (10^{-8} cm²/s), and the values for liquid metals (10^{-5} cm²/s).[46] For comparison, the calculated diffusion constant based on eq 6 for $E_{abs} = 1.16$ mJ/pulse ($T = 1100$ K) is $D \approx 10^{-10}$ cm²/s. We interpret this to mean that the particles are partially molten due to surface melting, and that the diffusion constant calculated above is an average over the solid and liquid portions of the particle. Moreover, the thickness of the fluid layer has to be

larger than the silver shell in order for the metals to inter-diffuse. Thus, surface melting at reduced temperatures is an important phenomena for both laser-induced reshaping and for inter-diffusion/alloying of metal nanoparticles.

V. Summary and Conclusions

The synthesis of bimetallic Au$_{core}$Ag$_{shell}$ and Ag$_{core}$Au$_{shell}$ nanoparticles using radiation chemistry has been demonstrated. The increase in the mean particle diameter agrees with that expected from the stoichiometry of the metal deposition. No separate nucleation took place during the deposition of the shell. However, the thickness of the deposited shell is not uniform among the particles. Laser-induced heating of the nanoparticles, mediated by the fast electron—phonon coupling process, produced melting and the consequent "erasing" of the core—shell geometry. This transformation of the abrupt metal—metal junction into a homogeneous alloyed nanoparticle reaches completion after many laser pulses. This implies that intermediate stages involving a graded interlayer are produced during the laser heating.

For nanosecond excitation, alloying occurs at absorbed energies of 5—6 mJ/pulse and fragmentation takes place at higher energies, $E_{abs} > 12$ mJ/pulse. In the case of 30 ps laser excitation, the thresholds for alloying and fragmentation are 1 and 4 mJ/pulse, respectively. For both excitation sources reshaping occurs at lower laser fluences than those needed for complete alloying. Calculations of the lattice temperatures based on the energy absorbed per pulse indicate that alloying and reshaping occur at much lower temperatures than the expected melting point. However, a more accurate calculation that properly accounts for the effects of heat transfer to the solvent, and how the different interfaces affect the phase transition temperatures, is required to fully understand the details of these processes. The observation that the thresholds for laser-induced transformations are lower for picosecond laser pulses compared to nanosecond laser pulses agrees with a recent study of laser-induced melting of Au nanorods by El-Sayed and co-workers.[27]

The spectral features of the core—shell nanoparticles are very different from those of the alloyed nanoparticles. Thus, these novel materials can in principle be used in all-optical data-storage devices, due to the contrast between the laser-melted particles ("written") and the nonirradiated nanoparticles that retain the core—shell structure.

References and Notes

(1) Ditlbacher, H.; Krenn, J. R.; Lamprecht, B.; Leitner, A.; Aussenegg, F. R. *Opt. Lett.* **2000**, *25*, 563.

(2) Ng, L. N.; Zervas, M. N.; Wilkinson, J. S.; Luff, B. J. *Appl. Phys. Lett.* **2000**, *76*, 1993.

(3) Mio, C.; Gong, T.; Terray, A.; Marr, D. W. M. *Rev. Sci. Instrum.* **2000**, *71*, 2196.

(4) Kamat, P. V.; Flumiani, M.; Hartland, G. V. *J. Phys. Chem. B* **1998**, *102*, 3123.

(5) Kurita, H.; Takami, A.; Koda, S. *Appl. Phys. Lett.* **1998**, *72*, 789.

(6) Takami, A.; Kurita, H.; Koda, S. *J. Phys. Chem. B* **1999**, *103*, 1226.

(7) Chang, S. S.; Shih, C. W.; Chen, C. D.; Lai, W. C.; Wang, C. R. C. *Langmuir* **1999**, *15*, 701.

(8) Safonov, V. P.; Shalaev, V. M.; Markel, V. A.; Danilova, Y. E.; Lepeshkin, N. N.; Kim, W.; Rautian, S. G.; Armstrong, R. L. *Phys. Rev. Lett.* **1998**, *80*, 1102.

(9) Fujiwara, H.; Yanagida, S.; Kamat, P. V. *J. Phys. Chem. B* **1999**, *103*, 2589.

(10) Niidome, Y.; Hori, A.; Sato, T.; Yamada, S. *Chem. Lett.* **2000**, 310.

(11) Link, S.; Burda, C.; Nikoobakht, B.; El-Sayed, M. A. *Chem. Phys. Lett.* **1999**, *315*, 12.

(12) Sato, T.; Kuroda, S.; Takami, A.; Yonezawa, Y.; Hada, H. *Appl. Organomet. Chem.* **1991**, *5*, 261.

(13) Mulvaney, P.; Giersig, M.; Henglein, A. *J. Phys. Chem.* **1993**, *97*, 7061.

(14) Sinzig, J.; Radtke, U.; Quinten, M.; Kreibig, U. *Z. Phys. D* **1993**, *26*, 242.

(15) Kreibig U.; Vollmer, M. *Optical Properties of Metal Clusters*; Springer: Berlin, 1995.

(16) Sinzig, J.; Quinten, M. *Appl. Phys. A* **1994**, *58*, 157.

(17) Liz-Marzán, L. M.; Philipse, A. P. *J. Phys. Chem.* **1995**, *99*, 15120.

(18) Treguer, M.; de Cointet, C.; Remita, H.; Khatouri, J.; Mostafavi, M.; Amblard, J.; Belloni, J.; de Keyzer R. *J. Phys. Chem. B* **1998**, *102*, 4310.

(19) Link, S.; Wang, Z. L.; El-Sayed, M. A. *J. Phys. Chem. B* **1999**, *103*, 3529.

(20) Link, S.; Burda, C.; Wang, Z. L.; El-Sayed, M. A. *J. Chem. Phys.* **1999**, *111*, 1255.

(21) Papavassiliou, G. C. *J. Phys. F* **1976**, *6*, L103.

(22) Enüstün, B. V.; Turkevich, J. *J. Am. Chem. Soc.* **1963**, *85*, 3317.

(23) Henglein, A.; Giersig, M. *J. Phys. Chem. B* **1999**, *103*, 9533.

(24) Henglein, A.; Meisel, D. *Langmuir* **1998**, *14*, 7392.

(25) Hodak, J. H.; Martini, I.; Hartland, G. V. *J. Phys. Chem. B* **1998**, *102*, 6958.

(26) Henglein, A.; Giersig, M. Manuscript in preparation.

(27) Link, S.; Burda, C.; Nikoobakht, B.; El-Sayed, M. A. *J. Phys. Chem. B* **2000**, *104*, 6152.

(28) Elsayed-Ali, H. E.; Juhasz, T.; Smith, G. O.; Bron, W. E. *Phys. Rev. B* **1991**, *43*, 4488.

(29) Sun, C. K.; Vallée, F.; Acioli, L. H.; Ippen, E. P.; Fujimoto, J. G. *Phys. Rev. B* **1994**, *50*, 15337.

(30) Groeneveld, R. H. M.; Sprik, R.; Lagendijk, A. *Phys. Rev. Lett.* **1995**, *51*, 11433.

(31) Ahmadi, T. S.; Logunov, S. L.; El-Sayed, M. A. *J. Phys. Chem.* **1996**, *100*, 8053.

(32) Logunov, S. L.; Ahmadi, T. S.; El-Sayed, M. A.; Khoury, J. T.; Whetten, R. L. *J. Phys. Chem. B* **1997**, *101*, 3713.

(33) Hodak, J. H.; Martini, I.; Hartland, G. V. *Chem. Phys. Lett.* **1998**, *284*, 135.

(34) Hodak, J. H.; Henglein, A.; Hartland, G. V. *J. Chem. Phys.* **2000**, *112*, 5942.

(35) Hodak, J. H.; Henglein, A.; Hartland, G. V. *J. Phys. Chem. B*, in press.

(36) Kakac, S.; Yenev, Y. *Heat Conduction*; Taylor and Francis: Washington, 1993.

(37) Ashcroft, N. W.; Mermin, N. D. *Solid State Physics*; Harcourt Brace: Orlando, 1976.

(38) Okamoto, H.; Massalki, T. B. *Binary Alloy Phase Diagrams*; ASM International: Ohio, 1990.

(39) Wautelet, M.; Dauchot, J. P.; Hecq, M. *Nanotechnology* **2000**, *11*, 6.

(40) Buffat, P.; Borel, J.-P. *Phys. Rev. A* **1976**, *13*, 2287.

(41) Wautelet, M. *J. Phys. D* **1991**, *24*, 343.

(42) Allen, G. L.; Bayles, R. A.; Gile, W. W.; Jesser, W. A. *Thin Solid Films* **1986**, *144*, 297.

(43) Ben David, T.; Lereah, Y.; Deutscher, G.; Kofman, R.; Cheyssac, P. *Philoso. Magn. A* **1995**, *71*, 1135.

(44) Wang, Z. L.; Petroski, J. M.; Green, T. C.; El-Sayed, M. A. *J. Phys. Chem. B* **1998**, *102*, 6145.

(45) Mohamed, M. B.; Wang, Z. L.; El-Sayed, M. A. *J. Phys. Chem. A* **1999**, *103*, 10255.

(46) Tu, K.-N.; Mayer, J. W.; Feldman, L. C. *Electronic Thin Film Science for Electrical Engineers and Materials Scientists*; Macmillan: New York, 1992.

(47) Tyrrell, H. J. V.; Harris, K. R. *Diffusion in Liquids*; Butterworth: London, 1984.